The Eddy-Driven Thermocline

PAOLA CESSI

Scripps Institution of Oceanography, University of California, San Diego, La Jolla, California

MAURIZIO FANTINI

ISAC-CNR, Bologna, Italy

(Manuscript received 15 July 2003, in final form 17 June 2004)

ABSTRACT

The role of baroclinic eddies in transferring thermal gradients laterally, and thus determining the stratification of the ocean, is examined. The hypothesis is that the density differences imposed at the surface by differential heating are a source of available potential energy that can be partially released by mesocale eddies with horizontal scales on the order of 100 km. Eddy fluxes balance the diapycnal mixing of heat and thus determine the vertical scale of penetration of horizontal thermal gradients (i.e., the depth of the thermocline). This conjecture is in contrast with the current thinking that the deep stratification is determined by a balance between diapycnal mixing and the large-scale thermohaline circulation. Eddy processes are analyzed in the context of a rapidly rotating primitive equation flow driven by specified surface temperature, with isotropic diffusion and viscosity. The barotropic component of the eddies is found to be responsible for most of the heat flux, and so the eddy transport is horizontal rather than isopycnal. This eddy transport takes place in the shallow surface layer where eddies, as well as the mean temperature, undergo diabatic, irreversible mixing. Scaling laws for the depth of the thermocline as a function of the external parameters are proposed. In the classical thermocline theory, the depth of the thermocline depends on the diffusivity, the rotation rate, and the imposed temperature gradient. In this study the authors find an additional dependence on the viscosity and on the domain width.

1. Introduction

In this study, we examine the role of baroclinic eddies in the heat balance of the deep ocean, in the region below the directly wind-driven thermocline. Unlike the atmosphere, which is heated ''internally'' by radiative processes, the ocean is differentially heated only at the top boundary and weakly by geothermal heating at the bottom. Thus, in statistical steady state, the total heat flux across every horizontal level satisfies (cf. Paparella and Young 2002)

$$\rho_0 C_p \langle wT - \kappa_T T_z \rangle = \langle Q_{\rm rad} e^{(z-H)/d} + Q_{\rm geo} \rangle. \qquad (1)$$

The angle brackets indicate a horizontal average over the domain. The first term on the right-hand side is the radiative heating, which decays away from the surface, $z = H$, on a depth scale d of about 4 m. The last term on the right-hand side is the geothermal heat flux. The balance of fluxes (1) is obtained by integrating the horizontally averaged heat equation vertically from the bottom to any level z. If the geothermal and molecular (proportional to κ_T) heat fluxes are neglected, the governing heat balance *at all levels* below the optical thickness d, is simply

$$\rho_0 C_p \langle wT \rangle = 0. \qquad (2)$$

At the same time, for an incompressible, hydrostatic fluid the vertical heat flux is related to the conversion C between potential energy (PE) and kinetic energy (KE) by the relation

$$C \equiv \rho_0^{-1} \langle \widetilde{\mathbf{u} \cdot \nabla p} \rangle = g\alpha \langle \widetilde{wT} \rangle, \qquad (3)$$

where $\mathbf{u}$ indicates the horizontal velocity, and the tilde indicates an average over all depths. Thus, the requirement that to a first approximation the horizontally averaged vertical heat flux vanishes at every level corresponds to a law of vanishing energy conversion. This constraint implies that the conversion C is a residual of much larger terms with different signs:

$$C = \underbrace{C_{\rm BW} + C_{\rm EP}}_{-} + \underbrace{C_{\rm MO} + C_{\rm BI}}_{+} + \cdots. \qquad (4)$$

Term $C_{\rm BW} < 0$ is the transfer from KE to PE that occurs when internal gravity waves break and overturn a stable stratification, thus raising the center of mass of the fluid. This contribution to C is often parameterized as downgradient diffusion with a diffusivity κ much larger than

Corresponding author address: Paola Cessi, UCSD-0213, La Jolla, CA 92093-0213.
E-mail: pcessi@ucsd.edu

the molecular value κ_T. Term $C_{\rm EP} < 0$ is the transfer from KE to PE that occurs when Ekman flux raises the center of gravity of the ocean by pushing down light fluid in the subtropical region and pulling up dense fluid in the subpolar region (e.g., Gill et al. 1974). Term $C_{\rm MO} > 0$ is the transfer from PE to KE due to large-scale meridional overturning: the center of gravity is lowered as dense water sinks in high latitudes and light water upwells elsewhere. Term $C_{\rm BI} > 0$ is the transfer from PE to KE due to baroclinic instability, which is the process analyzed in the present study. The ellipses in (4) indicate other transfers occurring at any of the scales intermediate between internal gravity wave overturns (10 cm) and mesoscale eddies (10^5 m).

Munk (1966) posits that diapycnal diffusion balances the large-scale upwelling associated with the production of deep water and high-latitude convection. In terms of (4) this corresponds to a two-term dominant balance $C_{\rm BW} + C_{\rm MO} \approx 0$, that is, a balance between processes at the two extremes of the spatial scales. An alternative view, at the origin of the process model formulated and analyzed here, is that $C_{\rm BW}$ is mainly balanced by $C_{\rm BI}$. This hypothesis does not imply that mean meridional circulation does not exist, just that its role in the conversions between KE and PE is subdominant.

The abyssal-recipe balance (Munk 1966) leads to a specific scaling for the stratification that is obtained by assuming that the time-mean meridional overturning circulation is characterized by a large-scale velocity $\overline{u}$, $\overline{v}$, and $\overline{w}$, which obeys the steady balance

$$\overline{u}\overline{T}_x + \overline{v}\overline{T}_y + \overline{w}\overline{T}_z \approx \kappa\overline{T}_{zz}, \tag{5}$$

where the overbar indicates a large scale and time average. Here temperature alone determines density. The transfer of KE to PE by breaking waves is parameterized as diapycnal diffusion, with diffusivity κ, and the isothermal surfaces are considered quasi horizontal so that diapycnal is synonymous with vertical.

With forcing confined to the surface and diffusion as the only means to transmit temperature gradients downward, the circulation is confined to a thermocline of thickness h, which according to (5) scales as

$$h = O\left(\frac{\kappa}{\overline{w}}\right). \tag{6}$$

Welander (1971) refined Munk's scaling by estimating the broad upwelling driven by differential surface heating. His scaling considers the meridional circulation $\overline{v}$ driven by the large-scale upwelling $\overline{w}$. The amplitude of $\overline{w}$ is set by the continuity equation,

$$\overline{v}_x + \overline{v}_y + \overline{w}_z = 0, \tag{7}$$

so that

$$\overline{w} = O\left(\frac{h\overline{v}}{L_y}\right). \tag{8}$$

Continents block the ocean flow to the east and west so that a large-scale east–west pressure gradient can be maintained. Thus we can assume that $\overline{v}$ is geostrophic and hydrostatic:

$$f\overline{v} \approx g\alpha\overline{T}_x \quad \text{or} \quad \frac{f\overline{v}}{h} \sim g\alpha\frac{\Delta T}{L_x}. \tag{9}$$

Eliminating $\overline{v}$ we arrive at Welander's estimate for the depth of the thermocline:

$$h = O\left(\frac{\kappa f L_x L_y}{g\alpha\Delta T}\right)^{1/3}. \tag{10}$$

For fixed surface density, ΔT is independent of κ, and therefore the depth of the thermocline and the meridional overturning are controlled by diffusion:

$$h \sim \kappa^{1/3} \quad \text{and} \quad h\overline{v} \sim \kappa^{2/3}. \tag{11}$$

In Welander's scaling, all density gradients, both vertical and horizontal, are confined to a thin diffusive surface boundary layer, and the zonally averaged meridional transport $h\nu$ decreases with κ.

Despite many dubious assumptions (chiefly that the longitudinal density differences are of the same order as the latitudinal density differences), these scalings of Welander have been confirmed by non-eddy-resolving numerical solutions of the primitive equations (Vallis 2000).

Essential to the scaling in (11) is the existence of an east–west pressure gradient that maintains a geostrophically balanced meridional flow. It is thus not obvious what happens when this balance fails in the circumpolar ocean because there are no boundaries at the east and west to support a pressure difference. It is also unclear how the balance is affected by time dependence.

In the following we show that without meridional boundaries the laminar (but unstable) flow obtained by differential surface heating is completely different: the horizontal density gradients penetrate all the way to the bottom so that there is no thermocline, the vertical stratification is everywhere weak, and a large zonal shear in thermal-wind balance results. However, this steady state is unstable to time-dependent perturbations, very similar to the classical Eady mode of baroclinic instability.

The ensuing baroclinic instability leads to a statistically steady thermal distribution that is qualitatively different from the laminar solution. In the equilibrium time-dependent state, the transport of heat, both meridional and vertical, is effected by the eddy fluxes, while the contribution of the mean meridional circulation is negligible.

The point of view that in a periodic geometry eddies must be important in setting up the stratification is not new: idealized simulations have found that indeed this is the case (Marshall et al. 2002; Karsten et al. 2002; Henning and Vallis 2004). Our study considers the extreme case where eddies alone, without a mean circulation, mantain the stratification against breaking gravity

TABLE 1. Parameter values used for the linear stability problem. Large values of κ and ν are chosen so that the boundary layers are well resolved.

Coriolis parameter	$f = 1 \times 10^{-4}$ s^{-1}
Mean density	$\rho_0 = 1 \times 10^3$ kg m^{-3}
Basin width	$L = 1 \times 10^6$ m
Basin depth	$H = 2000$ m
Gravity	$g = 10$ m s^{-2}
Vertical diffusivity	$\kappa = 4 \times 10^{-3}$ m^2 s^{-1}
Prandtl number	$\nu/\kappa = 10$
Surface temperature difference	$\Delta T = 2$ K
Surface temperature shape	$\Theta(y) = -\cos(2\pi y/\mathrm{L})$
Coefficient of thermal expansion	$\alpha = 2 \times 10^{-4}$ K^{-1}

waves. Our process model enables us to investigate the hypothesis, complementary to that of Munk (1966) and Welander (1971), that mesoscale eddies, rather than the mean flow, balance small-scale vertical mixing.

2. The model

If haline effects are ignored, the buoyancy-driven circulation is described by the primitive equations:

$$\begin{aligned} u_t + uu_x + vu_y + wu_z - fv &= -p_x/\rho_0 + \nu u_{zz} + \nu\nabla^2 u + \nu_6\nabla^6 u, \\ v_t + uv_x + vv_y + wv_z + fu &= -p_y/\rho_0 + \nu v_{zz} + \nu\nabla^2 v + \nu_6\nabla^6 v, \\ p_z &= g\rho_0\alpha T, \\ u_x + v_y + w_z &= 0, \quad \text{and} \\ T_t + uT_x + vT_y + wT_z &= \kappa T_{zz} + \kappa\nabla^2 T + \nu_6\nabla^6 T. \end{aligned} \tag{12}$$

Hereinafter, ∇^2 denotes the two-dimensional, horizontal Laplacian. Sixth-order hyperdiffusion and hyperviscosity with the same coefficient, ν_6, are included to limit the noise at the smallest resolved scale. The boundary conditions (b.c.) are

$$\begin{aligned} w = u_z = v_z = 0 \quad &\text{at } z = H, \\ w = u = v = 0 \quad &\text{at } z = 0, \\ T = \Delta T\Theta(y) \quad &\text{at } z = H, \quad \text{and} \\ T_z = 0 \quad &\text{at } z = 0. \end{aligned} \tag{13}$$

The shape of the temperature distribution, $\Theta(y)$, is given in Table 1. Our choice of a prescribed temperature distribution at the surface, rather than a fixed flux, is close to the oceanic situation where the mixed layer temperature is rapidly relaxed to an apparent atmospheric temperature.

For the sake of simplicity, we assume the Coriolis parameter f to be constant. Moreover we take all variables to be periodic in x and y so that lateral friction and diffusion can be made small without having to resolve thin side boundary layers, for example $T(x, y, z, t) = T(x + L, y, z, t) = T(x, y + L, z, t)$. Here, ν and κ are viscosity and diffusivity due to unresolved small-scale processes, such as internal gravity waves.

There are four nondimensional parameters controlling the system: the thermal Rossby number Ro, the Prandtl number Pr, the Ekman number Ek, and the aspect ratio H/L. The definitions are

$$\mathrm{Ro} \equiv \frac{g\alpha\Delta T H}{f^2 L^2}, \quad \mathrm{Pr} \equiv \frac{\nu}{\kappa}, \quad \text{and} \quad \mathrm{Ek} \equiv \frac{1}{H}\sqrt{\frac{\nu}{f}}. \tag{14}$$

In order to understand how mesoscale eddies and diapycnal mixing interact, we purposefully exclude several processes that are of importance in ocean. Specifically, we ignore the mechanical forcing and Ekman pumping imparted by the wind stress. In the subtropical oceans, the downward Ekman pumping is the primary process that pushes the surface density gradients into the upper ocean (Luyten et al. 1983): this is the term C_{EP} in (4). Diapycnal mixing plays an important role below the ''ventilated thermocline'' (Stommel and Webster 1962; Young and Ierley 1986; Salmon 1990; Samelson and Vallis 1997), and our process study is relevant to this deep region.

In the subpolar regions, where the Ekman pumping is upward, ventilation cannot occur and diapycnal mixing is essential for deepening the density gradient below the surface. In this case, eddy processes such as those described in our study are an important participant in the ensuing balance.

Without lateral boundaries wind-driven gyres are not possible, but the wind stress still generates Ekman flow, whose mean meridional heat transport is largely cancelled by the eddy heat transport (Doos and Webb 1994; Karsten et al. 2002). This scenario is appropriate for the Antarctic Circumpolar Current. In this case, the ''residual circulation,'' equal to the sum of the mean and eddy-induced heat transport, balances the diabatic terms in the heat equation. The process model formulated here deliberately eliminates the mean meridional circulation by ignoring the wind stress and the lateral boundaries so that the eddy heat transport directly balances the diabatic sources.

The problem formulated in (12) and (13) is the simplest process model that enables us to study the role of eddies in the formation of the thermocline.

3. The symmetric steady state

In this section we show that a *laminar* thermocline cannot be supported by the model formulated in (12).

In a periodic geometry, for x-independent buoyancy forcing and excluding for the moment the spontaneous generation of x-dependent instabilities, we can solve (12) and (13) by taking $\partial_x = 0$. Thus the longitudinal pressure gradient vanishes so that the meridional flow is frictionally, rather than geostrophically, balanced. In

the following we show that this restriction leads to a weak meridional transport.

Since $u_x = 0$, it is useful to describe the meridional and vertical flow by a streamfunction ψ such that

$$v = -\psi_z \quad \text{and} \quad w = \psi_y. \tag{15}$$

The symmetric steady momentum equations then become (neglecting hyperviscosity and horizontal viscosity, both small when $H \ll L$)

$$J(\psi, fy - u) = \nu u_{zz} \quad \text{and}$$

$$-J(\psi, \psi_z) + fu = -\frac{p_y}{\rho_0} + \nu v_{zz},$$

where $J(A, B) \equiv A_y B_z - B_y A_z$.

a. Scaling

Because Ro $\ll 1$, the zonal flow u is essentially in thermal wind balance and the angular momentum, $fy - u$, is dominated by the planetary term. Specifically, we have

$$-fv = \nu u_{zz} + O(\text{Ro}) \quad \text{and} \tag{16}$$

$$fu = -\frac{p_y}{\rho_0} + \nu v_{zz} + O(\text{Ro}). \tag{17}$$

Using the values in Table 1, Ro $= 8 \times 10^{-4}$.

Using the definition of the streamfunction, (16) can be integrated once to give

$$f\psi = \nu u_z. \tag{18}$$

This relation shows that, in order for ψ to vanish at both the top and bottom boundaries, we must require $u_z = 0$ at $z = 0$ (''no stress''), as well as imposing the no-slip condition. With the aid of the hydrostatic relation and of (17) we obtain a single equation for ψ:

$$f^2\psi + \nu^2\psi_{zzzz} = -\nu\alpha g T_y. \tag{19}$$

We are now in a position to estimate that the order of magnitude of ψ is

$$\psi = O\left(\frac{g\alpha\Delta T\nu}{f^2 L}\right). \tag{20}$$

Because ψ is proportional to the small viscosity ν, it is not surprising that the steady symmetric temperature, governed by

$$J(\psi, T) = \kappa T_{zz} + \kappa T_{yy}, \tag{21}$$

is dominated by vertical diffusion rather than advection. Specifically we have

$$\frac{\psi_y T_z}{\kappa T_{zz}} = O(\text{RoPr}) \ll 1. \tag{22}$$

Because of the small aspect ratio, $H \ll L$, and of isotropic diffusion, the horizontal diffusion is also negligible at leading order in (21). We thus define a small parameter, $\epsilon \equiv$ RoPr, and expand the temperature in powers of ϵ:

$$T = \Delta T(\theta_0 + \epsilon\theta_1) + O(\epsilon^2). \tag{23}$$

b. The leading-order temperature

The leading-order temperature satisfies

$$\theta_{0zz} = 0 \quad \text{and} \quad \theta_{0z} = 0 \quad \text{at } z = 0, \quad \text{and}$$

$$\theta_0 = \Theta(y) \qquad \text{at } z = H. \tag{24}$$

The solution is simply

$$\theta_0(y, z) = \Theta(y) \tag{25}$$

so that the leading-order temperature is vertically homogenous and equal to the imposed surface distribution. This result should be compared with the numerical calculations of Vallis (2000 cf. his Fig. 9), which show vertically homogeneous temperature in the zonally reentrant portion of the computational domain. Thus, there is no thermocline in the laminar solution, and Welander's scaling (10) does not apply in a reentrant geometry.

c. The leading-order velocity

The leading-order pressure p_0 that drives the velocity field is given by

$$p_0 = \rho_0 g\alpha\Delta T\Theta(y)[z - P(y)], \tag{26}$$

where $P(y)$ is proportional to the barotropic component of the pressure. The unknown $P(y)$ is determined below by imposing the no-stress constraint at the bottom boundary, as required by mass conservation.

We introduce a complex function, $\chi \equiv u + iv$, which is governed by

$$f\chi = -g\alpha\Delta T\Theta_y(z - P) - i\nu\chi_{zz}. \tag{27}$$

The solution that satisfies no-stress ($\chi_z = 0$) at $z = H$ and no-slip ($\chi = 0$) at $z = 0$ is

$$\chi = \frac{g\alpha\Delta T}{f}\Theta_y(P - z + \delta F^+ - PF^-). \tag{28}$$

We have defined the depth of the Ekman layer, $\delta \equiv \sqrt{2\nu/f}$, and the boundary layer corrections

$$F^+(z/\delta) \equiv (1 + i)^{-1}e^{(1+i)(z-H)/\delta} \quad \text{and}$$

$$F^-(z/\delta) \equiv e^{-(1+i)z/\delta}. \tag{29}$$

The additional boundary condition $u_z = 0$ at $z = 0$ determines the barotropic pressure:

$$P(y) = \delta. \tag{30}$$

We can now calculate ψ using (18) and find

$$\psi = -\frac{g\alpha\Delta T\nu}{f^2}\Theta_y \text{Re}[1 - (1 + i)(F^+ + F^-)]. \tag{31}$$

The meridional overturning thus calculated is shown in Fig. 1.

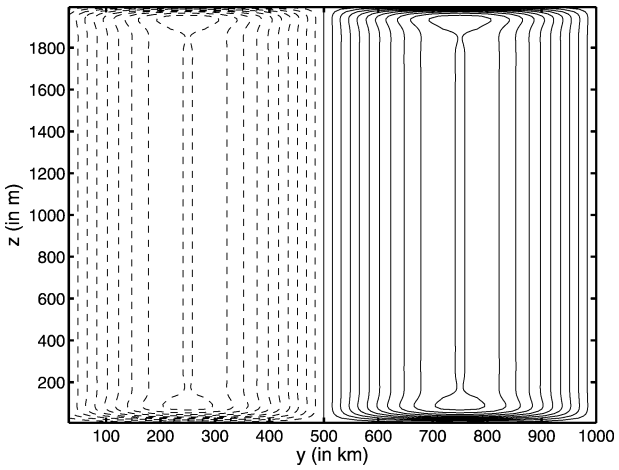

FIG. 1. The leading-order streamfunction in the (y, z) plane. The parameter values are given in Table 1. Positive contours are solid, and negative contours are dashed. The contour interval is 0.01 $m^2\ s^{-1}$.

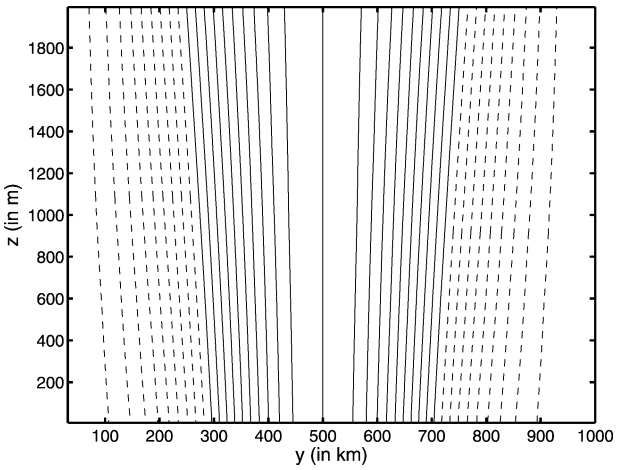

FIG. 2. The first two terms in the Ro expansion of the temperature in the y, z plane. The parameter values are given in Table 1. Positive contours are solid, and negative contours are dashed. The contour interval is 0.2°C.

The zonal velocity is given by the real part of (28) and it is much larger than the meridional velocity (the maximum of $\overline{u}$ is 0.5 m s^{-1}). The zonal velocity is characterized by a large interior vertical shear, the stability of which is examined in the next section.

d. The stratification

The leading-order temperature is vertically homogeneous, and yet the weak meridional circulation provides for a weak vertical stratification, determined by the $O(\epsilon)$ correction to the temperature θ_1, which satisfies

$$-\psi_z\theta_{0y} = \kappa\theta_{1zz} \quad \text{and} \quad \theta_{1z} = 0 \quad \text{at } z = 0, \quad \text{and}$$
$$\theta_1 = 0 \qquad \text{at } z = H, \tag{32}$$

with ψ given by (31). We can immediately integrate (32) vertically using the bottom b.c. to find the stratification

$$\kappa\theta_{1z} = -\psi\theta_{0y}. \tag{33}$$

Integrating once more in the vertical and using the top b.c. we find

$$\theta_1 = \mathrm{Pr}\frac{g\alpha\Delta T}{f^2}\Theta_y^2[z - H + \delta\mathrm{Re}(F^+ - F^- - 1)]. \tag{34}$$

Thus, we can write the dimensional temperature field as

$$T(y, z) = \Delta T\Theta(y) + \Delta T\theta_1(y, z) + O(\epsilon^2). \tag{35}$$

The Richardson number, $\mathrm{Ri} \equiv N^2/u_z^2$ with $N^2 \equiv g\alpha T_z$, is simply

$$\mathrm{Ri} = \mathrm{Pr}. \tag{36}$$

Figure 2 shows the temperature in (35) using the parameter values of Table 1.

Notice that, although the Rossby number is small, we are far from the quasigeostrophic limit, which is recovered when the Richardson number, and thus the Prandtl number, are $O(\mathrm{Ro}^{-2})$. For a Prandtl number $O(1)$, the stratified part of the temperature, contained in θ_1, is much smaller than the horizontally varying part of the temperature in θ_0. Thus the laminar flow does not have a thermocline.

In summary, the rapidly rotating symmetric flow is weakly stratified in the vertical (Fig. 2): essentially, the weak dissipation leads to a meridional overturning, independent of κ but proportional to ν (cf. Fig. 1). The meridional circulation turns the horizontal temperature gradients into vertical gradients through the balance in (32) and thus establishes a weak stratification. Remarkably the Richardson number is equal to the Prandtl number.

Neglecting the thin Ekman layers at the top and bottom, the steady, symmetric state is given by

$$T \approx \Delta T\Theta(y) + \mathrm{Pr}\frac{\alpha g}{f^2}(\Delta T\Theta_y)^2(z - H),$$

$$u \approx \frac{g\alpha\Delta T}{f}\Theta_y(\delta - z), \quad \text{and} \quad \psi \approx -\frac{g\alpha\Delta T\nu}{f^2}\Theta_y.$$

While unrealistic, Fig. 2 describes the weakly stratified density structure found in the Antarctic Circumpolar Current regions of non-eddy-resolving ocean models (e.g., Vallis 2000).

Because of the strongly vertically sheared zonal flow, and nearly vertical isopycnals, this symmetric state must be prone to baroclinic instabilities that break the zonal homogeneity, release available potential energy, and decelerate the mean zonal velocity.

4. Linear stability analysis

To illustrate the instability of the basic state discussed in the previous section, we now examine the case where

Θ_y is constant; that is, $\overline{T}_y = -\Delta T/L$. We regard this as a local approximation of the latitudinally varying basic state (35) valid when the scale of the unstable waves is much smaller than L.

With this uniform thermal gradient the approximate solution (35) becomes an exact steady state of the nonlinear primitive equations (12). (Higher-order terms in the expansion, involving Θ_{yy}, are all zero.) Thus we write

$$(u, v, w, p, T) = (\overline{u}, \overline{v}, \overline{w}, \overline{p}, \overline{T}) + (u', v', w', p', T'), \quad (37)$$

where the overbar indicates the steady, x-independent basic state and the primes are time- and x-dependent perturbations. The basic state is given by

$$\overline{T} = -\Delta T\frac{y}{L} + \frac{\overline{N}^2}{g\alpha}[z - H - \delta \mathrm{Re}(F^+ - F^- - 1)],$$

$$\overline{u} + i\overline{v} = -\frac{g\alpha\Delta T}{fL}[\delta - z + \delta(F^+ - F^-)], \quad \text{and}$$

$$\overline{w} = 0. \quad (38)$$

We have defined the interior constant stratification $\overline{N}^2$ as

$$\overline{N}^2 \equiv \mathrm{Pr}\frac{(g\alpha\Delta T)^2}{f^2L^2}. \quad (39)$$

Except for corrections confined to thin Ekman layers, (38) is the basic state for the Eady problem, with every quantity related to the imposed surface gradient, $\Delta T/L$.

For simplicity, we restrict all fields of the linear perturbations to be independent of y so that $u'_x + w'_z = 0$. (In the classic Eady problem, the most unstable disturbances have this structure.) With this choice we can introduce a streamfunction ϕ, such that

$$u' = \phi_z \quad \text{and} \quad w' = -\phi_x. \quad (40)$$

It is then possible to eliminate the pressure in favor of the temperature by taking the z derivative of the zonal momentum equation so that the perturbation fields are governed by the following linearized system:

$$\phi_{zzt} + \overline{u}\phi_{xzz} - \overline{u}_{zz}\phi_x - f v'_z = -\alpha g T'_x + \nu\phi_{zzzz}, \quad (41)$$

$$v'_t + \overline{u}v'_x - \overline{v}_z\phi_x + f\phi_z = \nu v'_{zz}, \quad \text{and}$$

$$T'_t + \overline{u}T'_x + v'\overline{T}_y - \phi_x\overline{T}_z = \kappa T'_{zz}. \quad (42)$$

The boundary conditions are

$$\phi = \phi_z = v' = 0 \quad \text{at } z = 0,$$

$$\phi = \phi_{zz} = v'_z = 0 \quad \text{at } z = H,$$

$$T' = 0 \quad \text{at } z = H, \quad \text{and}$$

$$T'_z = 0 \quad \text{at } z = 0.$$

Except for the top and bottom boundary layers in the basic state and for the temperature and velocity boundary conditions, the stability problem is rather similar to the classical Eady model (Eady 1949; Stone 1966).

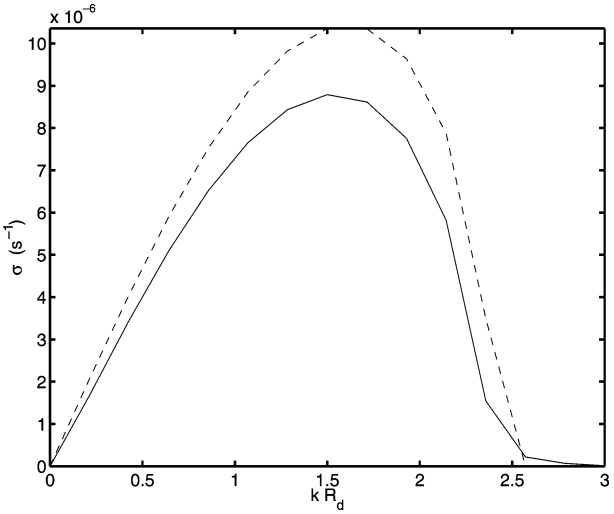

FIG. 3. The growth rate as a function of kR_d (solid line), and the quasigeostrophic prediction using the interior inviscid basic state (dashed line). The parameter values are in Table 1, giving $R_d \approx 2.5$ km.

We seek solutions of the modal form

$$(\phi, v', T') = [\mathbf{\Phi}(z), \mathbf{V}(z), \mathbf{T}(z)]e^{ikx+(\sigma+i\omega)t}. \quad (43)$$

This *ansatz* results in an eigenproblem where $[\mathbf{\Phi}(z), \mathbf{V}(z), \mathbf{T}(z)]$ is the eigenfunction and $\sigma + i\omega$ is the eigenvalue. We solve the eigenproblem numerically using the package developed by Weideman and Reddy (2000).

Figure 3 shows the growth rate σ as a function of the wavenumber multiplied by the deformation radius kR_d (solid line). We have denoted the deformation radius with

$$R_d \equiv \overline{N}H/f, \quad (44)$$

where $\overline{N}$ is defined in (39). Also shown is the growth rate σ_{QG} predicted by the inviscid, nondiffusive quasigeostrophic approximation with the same basic state. From Gill (1982),

$$\sigma^2_{\mathrm{QG}} = \frac{f^2}{\overline{N}^2}\overline{u}_z^2\left[\frac{kR_d}{2}\tanh\left(\frac{kR_d}{2}\right) - 1\right] \times \left[\frac{kR_d}{2}\coth\left(\frac{kR_d}{2}\right) - 1\right]. \quad (45)$$

Despite the weak stratification and the boundary layers, the quasigeostrophic prediction is rather good.

Figure 4 shows a snapshot of the perturbation temperature T' of the fastest-growing mode. The familiar pattern of eastward tilt with height is only changed in a thin diffusive boundary layer at the top. Thus small diffusion and viscosity do not alter the qualitative mechanism of baroclinic instability.

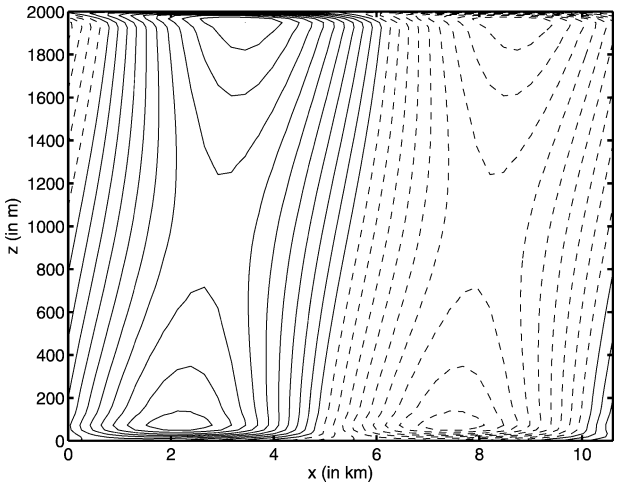

FIG. 4. A snapshot of the temperature perturbation for the fastest-growing mode.

5. Nonlinear equilibration and the statistical steady state

We now numerically simulate the process model formulated in (12) and (13) using the surface condition $T = -\Delta T \cos(2\pi y/L)$. We expect the eddies to transport heat latitudinally, to release the available potential energy, and to rearrange the zonally and time-averaged density field by establishing a zonally averaged thermocline whose properties depend on the statististics of the eddy field. Our approach is to perform eddy-resolving numerical simulations of the primitive equations (12) described in section 2. We employ a variable-grid, finite-difference model with $N \times N$ grid points in the horizontal plane (N is either 128 or 256) and enough vertical points to resolve the top and bottom Ekman layers (the details are in appendix A).

The f-plane domain has horizontal dimensions $L = 1000$ km in both directions and all variables are periodic in x and y. At the rigid surface, $z = H$, we specify the temperature and require no stress. At the rigid bottom, $z = 0$, we impose no flux of heat and no slip. The diffusivity κ and the viscosity ν are isotropic in all three dimensions. Our choice of isotropic diffusivity is unconventional, but it ensures that no hidden diapycnal fluxes occur except at the very small scales where hyperdiffusion is active. Furthermore, when eddy processes are directly resolved, there is no need for an augmented diffusivity in the isopycnal direction. With isotropic viscosity, lateral friction is generally negligible, and dissipation occurs through the vertical component of viscosity and the hyperviscosity (more details are given in appendix A).

No convective adjustment is applied because this choice is the only one that guarantees an unambiguous dependence of the results on the diffusivity. However, unstable stratification develops below the regions where the coldest temperatures are prescribed. In general, an unstable mean stratification below the cooled regions is not surprising since convective plumes entrain warmer surrounding fluid as they descend. When convective plumes are well resolved, the entrainment occurs over localized regions and the time-averaged bottom temperature is close to the minimum surface temperature. With the limited resolution used in the model the unstably stratified regions are substantial, but we feel this is a small price to pay in exchange for knowing the value of the vertical diffusivity everywhere and for having a well-defined energy balance. Also, as discussed in section 9, the bottom temperature decreases as horizontal resolution is increased, reassuring us that hydrostatic convection is occurring, albeit limited by the discretization.

The goal of the simulations is to establish the dependence on the external parameters of various quantities characterizing the statistically steady fields. Specifically, we wish to examine the depth of penetration of the surface temperature gradients as a function of the diffusivity κ, of the viscosity ν, of the temperature difference ΔT, and of the oceanic depth H or, alternatively, in terms of the four nondimensional parameters, Ro, Pr, Ek, and H/L.

A typical snapshot (Fig. 5) of the instantaneous temperature below the thermocline reveals that at depth the stirring by the eddy field alters qualitatively the structure imposed at the surface. Although the surface temperature gradients are concentrated near the latitudes $y = 250$ km and $y = 750$ km, the fluctuations are approximately uniformly distributed throughout the domain.

Hereinafter, we indicate with an overbar the zonal average, for example,

$$\overline{T}(y, z, t) \equiv L^{-1} \int_0^L T(x, y, z, t)\, dx, \tag{46}$$

and with angle brackets the horizontal average, for example,

$$\langle T \rangle \equiv L^{-2} \int_0^L \int_0^L T\, dx\, dy. \tag{47}$$

The hallmark of the statistically steady state established by the eddy fluxes is a zonally averaged temperature $\overline{T}$, with a shallow thermocline as illustrated in Fig. 6. The parameter values are as in Table 1 except that Pr = 50 and $\kappa = 8 \times 10^{-4}$. The zonally averaged temperature field differs qualitatively from that of the steady symmetric solution described in section 3 and shown in Fig. 2: here the horizontal temperature gradients are confined to a distinctive thermocline region, much shallower than the depth of the domain.

The zonally averaged temperature is maintained by a balance between vertical diffusion and convergence of eddy heat transport:

$$(\overline{v'T'})_y + (\overline{w'T'})_z \approx \kappa \overline{T}_{zz}. \tag{48}$$

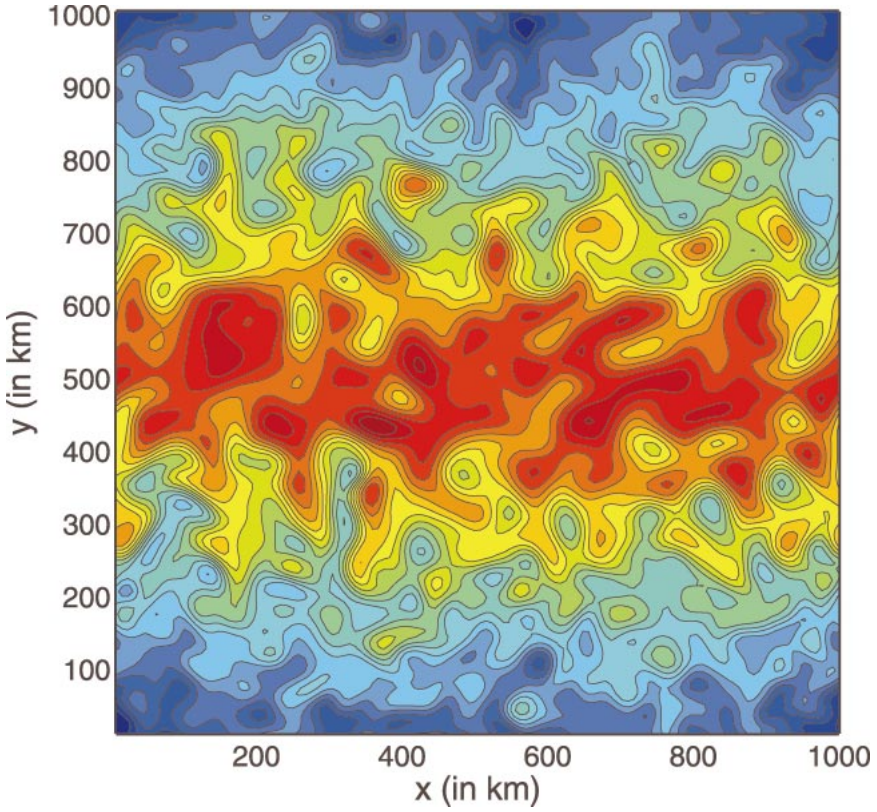

FIG. 5. A snapshot of the temperature T at $z = 1314$ m for $\kappa = 8 \times 10^{-4}$ m^2 s^{-1} and Pr = 50. At this depth the eddy field dominates over the zonal mean. The contour interval is 0.018°C and the range is from −1.11° to −1.48°C. All the other parameters are as in Table 1.

The contribution to the heat transport by the zonally averaged circulation, $(\overline{v}\,\overline{T})_y + (\overline{w}\,\overline{T})_z$, is nonzero but much smaller than the eddy counterpart. Thus, (48) is a very good approximation.

There are two separate components of the mean temperature field: the horizontally averaged temperature $\langle T\rangle(z)$ and the meridionally varying mean temperature $\theta(y, z) = \overline{T} - \langle T\rangle$; $\langle T\rangle$ and θ obey different dynamics:

$$(\overline{v'T'})_y \approx \kappa\theta_{zz} \quad \text{and} \tag{49}$$

$$\langle wT\rangle = \kappa\langle T\rangle_z. \tag{50}$$

In steady state, (50) is the exact result (2), stating that *at every depth* the horizontally averaged vertical heat flux vanishes, a consequence of imposing no flux at the bottom. As shown in Fig. 7, the vertical flux due to advection is dominated by the eddy component, $\langle wT\rangle \approx \langle w'T'\rangle$, while the heat transport by the zonally

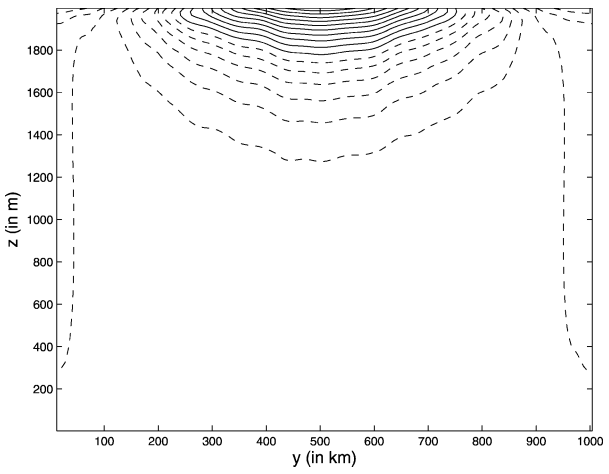

FIG. 6. The zonally averaged temperature $\overline{T}$ for $\kappa = 8 \times 10^{-4}$ m^2 s^{-1} and Pr = 50 as a function of y and z. The contour interval is 0.2°C and negative values are dashed. All other parameters are as in Table 1.

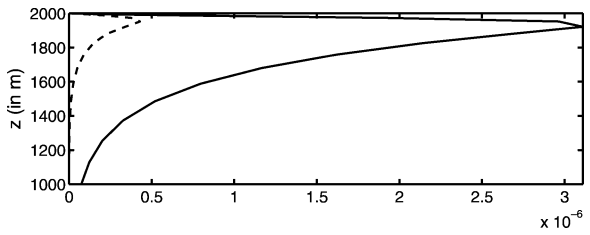

FIG. 7. The eddy $\langle w'T'\rangle$ (solid) and zonal mean $\langle \overline{w}\,\overline{T}\rangle$ (dashed) contributions to the area-averaged vertical flux of temperature as a function of depth (only the top half of the domain is shown). All parameters are as in Fig. 6.

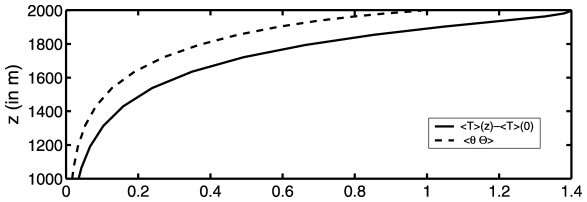

FIG. 8. The solid line shows $\langle T\rangle(z) - \langle T\rangle(0)$ and the dashed line is $\langle \theta\, \Theta\rangle$ as a function of z for the parameters of Fig. 6. The shape of the surface temperature is $\Theta = -\cos(2\pi y/L)$. Only the top half of the domain is shown.

averaged meridional circulation is negligible. Moreover, according to (50), the vertical eddy flux is up the mean gradient.

Our principal focus is on $\theta(y, z)$ since the vertical structure of $\langle T\rangle$ depends on secondary circulation of the eddies and on the resolved convection, whose dependence on external parameters is very indirect. The balance (49) neglects the vertical eddy flux convergence, which is found to be much smaller than the lateral component as detailed in section 6. Figures 8 and 9 show the two components of the zonally averaged temperature for the calculation of Fig. 6. Remarkably, θ is almost a separable function of y and z so that the surface temperature distribution Θ is reproduced at depth with decreasing amplitude:

$$\theta(y, z) = \Delta T \Theta(y)\vartheta(z), \tag{51}$$

where $\Theta \equiv -\cos(2\pi y/L)$. Figure 8 compares $\langle T\rangle$ (solid line) with the projection of θ on the surface temperature (dashed line) showing that the two profiles roughly follow each other. Given the simple structure of θ it is natural to define the depth of the thermocline as

$$h \equiv \left(\int_0^H \langle\theta^2\rangle\, dz \Big/ \int_0^H \langle\theta_z^2\rangle\, dz\right)^{1/2}. \tag{52}$$

For the field in Fig. 6 $h = 189$ m. A number of alternative definitions, which would be equivalent for a single-scale exponential, are possible, but they do not modify the following discussion. The depth of the mean thermocline, h defined in (52), is determined by the heat flux produced by the eddies, whose statistics must be established.

The partition of $\overline{T}(y, z)$ between $\theta(y, z)$ and $\langle T\rangle(z)$ also reveals that the mean state obtained here is far from the quasigeostrophic limit because the horizontal temperature differences are larger than the vertical ones.

A snapshot of the meridional eddy flow, shown in Fig. 10, reveals that, although the mean temperature gradients are confined to a surface layer, the perturbation velocity reaches all the way to the oceanic bottom. It is well established that in the quasigeostrophic, two-layer case, the eddy heat flux is completely carried by the barotropic component of the velocity (Salmon 1980; Larichev and Held 1995). The heat flux produced by the baroclinic component is small because the temperature gradient and the baroclinic velocity are approximately orthogonal by thermal wind balance. Thus, in the two-layer case, the temperature is advected as a passive scalar by the barotropic flow. This motivates us to examine whether the same property holds in our continuously stratified case. We thus partition the flow in a barotropic component, defined as the vertical average, and a baroclinic part, defined as the residual from the vertical average and advect a passive scalar with the barotropic component of the velocity.

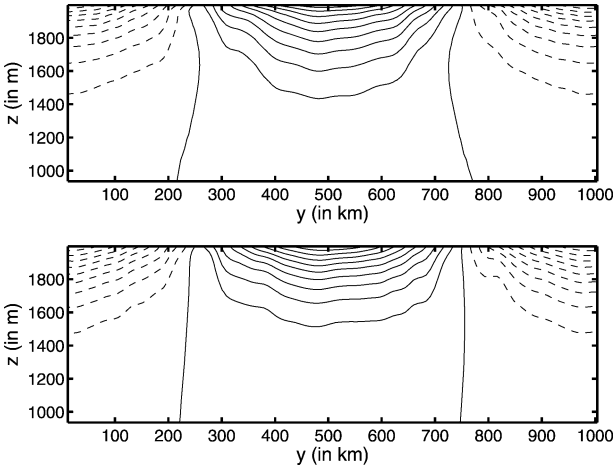

FIG. 9. (top) Temperature θ as a function of y and z for the parameters of Fig. 6. (bottom) The zonally averaged passive scalar, $\overline{S}(y, z)$, advected by the barotropic component of the velocity. Only the top half of the domain is shown. The contour interval is 0.2°C, and negative values are dashed.

6. A scalar advected by the barotropic flow

The field $\theta(y, z)$ compares very well to that obtained by evolving a passive scalar identically forced at the surface and subject to the same diffusivity but

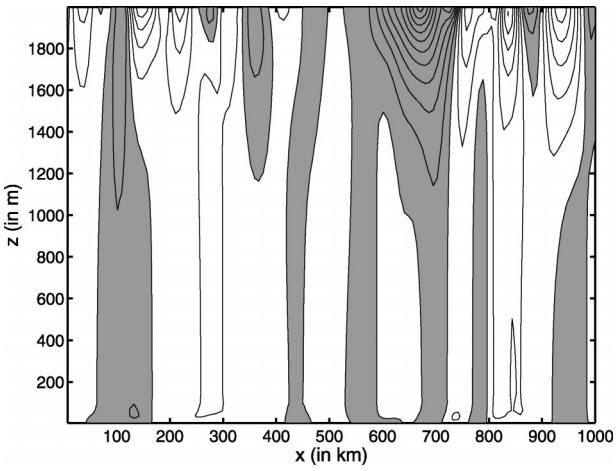

FIG. 10. A snapshot of v for a section along $y = L/4$ illustrates that the velocity does not change sign in the vertical direction and thus has a pronounced barotropic component.

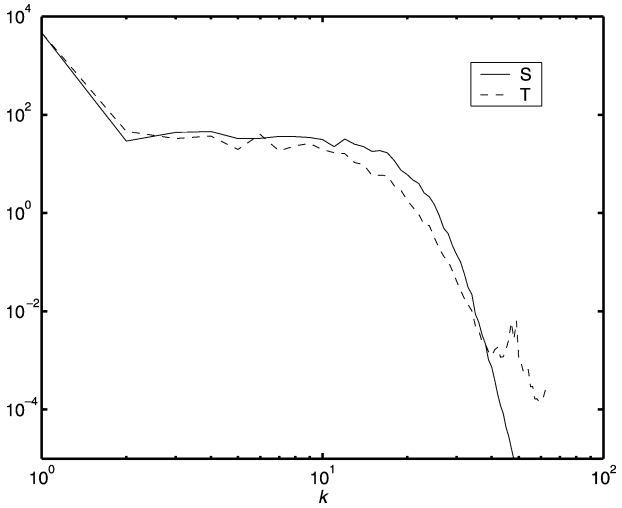

FIG. 11. The spectra of T (dashed) and S (solid) for the simulation shown in Fig. 9 at $z = 1895$ m. This is a representative depth, and the spectra at other levels exhibit a similar agreement.

advected *only by the vertically averaged* velocities, $(U, V) \equiv H^{-1}\int_0^H (u, v)\, dz$. The zonal average of the passive scalar, $\overline{S}(y, z)$, is shown in the bottom panel of Fig. 9 and compared with $\overline{\theta}(y, z)$ (top panel). The two fields are almost identical. This result suggests that the baroclinic eddy velocity is well represented by a single vertical structure. Consequently, from thermal wind balance, the baroclinic velocities are largely orthogonal to the temperature gradient and transport no heat.

To examine the fluctuations we define spectra $\mathcal{T}$ and $\mathcal{S}$, so that

$$\langle (T - \langle T\rangle)^2(x, y, z, t)\rangle = \int_0^\infty \mathcal{T}(k, z, t)\, dk \quad \text{and} \tag{53}$$

$$\langle S^2(x, y, z, t)\rangle = \int_0^\infty \mathcal{S}(k, z, t)\, dk. \tag{54}$$

Figure 11 shows that $\mathcal{S}$ is almost identical to $\mathcal{T}$. Thus T and S also exhibit the same variance at all scales and all depths. Evidently, temperature fluctuations are largely independent of $\langle T\rangle$ since the latter does not enter either the evolution of the scalar or of the horizontal momentum. This result justifies our focus on the horizontally varying part of the temperature.

The scalar model shows that the barotropic eddy velocities determine both $\theta(y, z)$ and the temperature fluctuations. We thus proceed with a deeper study of the scalar model, using variance budgets.

With the Reynolds decomposition, $S = \overline{S} + S'$, the scalar fluctuations satisfy

$$\overbrace{S'_t}^{O(S'/t_{\text{eddy}})} + \overbrace{\overline{U}S'_x}^{O(VS'/l)} + \overbrace{V'\overline{S}_y}^{O(V'\overline{S}/L)} = \overbrace{\kappa S'_{zz}}^{O(\kappa S'/h^2)} + O(V'S'), \tag{55}$$

while the mean field is governed by

$$(\overline{V'S'})_y = \kappa \overline{S}_{zz}. \tag{56}$$

In (55) we have assumed that the fluctuations, S', are well described by linear dynamics. We have denoted with t_{eddy} and l the time and length scales of the scalar fluctuations. The scalar variance equation obtained from (55) then reads

$$\overline{V'S'}\,\overline{S}_y = \kappa \overline{S'S'_{zz}}. \tag{57}$$

Vertical integration of (57) gives

$$\int_0^H \overline{V'S'}\,\overline{S}_y\, dz = -\kappa \int_0^H \overline{S'^2_z}\, dz. \tag{58}$$

The scalar variance integral in (58) indicates that the sense of the eddy flux is generally down the mean gradient, although not necessarily so at every depth.

A scaling relation between S' and $\overline{S}$ can be found by eliminating the eddy transport between (56) and (57):

$$\left(\frac{\overline{S'S'_{zz}}}{\overline{S}_y}\right)_y = \overline{S}_{zz}. \tag{59}$$

The balance (59) shows that S'_z (and therefore T'_z) is of the same order as $\overline{S}_z$ (and therefore θ_z). In this surface layer S' (but not its vertical derivatives) is especially small, since it must vanish at the surface, so that the dominant balance in (55) is

$$V'\overline{S}_y \approx \kappa S'_{zz}. \tag{60}$$

This balance indicates that the vertical scale of the fluctuations, S' (and therefore of T'), is of the same order as the vertical scale of the zonal average, $\overline{S}$ (and therefore of θ), a result confirmed by the numerical simulations. Because of (59), it follows that the amplitude of the fluctuations is of the same order as the amplitude of the zonal average, a result in contrast with the traditional mixing length arguments of turbulence, where the horizontal *gradients* of the eddy and of the mean have the same amplitude.

Because of (60) and (59) the vertical scale h is determined by

$$h \sim (\kappa L/V')^{1/2}. \tag{61}$$

Thus, to complete the scaling of the thermocline depth we must provide a scaling for the amplitude of the barotropic eddies, V' in (61), which is done in the next section.

The success of the scalar model and the importance of the barotropic component of the eddies indicate that within the diffusive thermocline the eddy heat flux is predominantly *horizontal*, rather than isopycnal. The quantitative agreement between the spectra of the scalar and temperature perturbation demonstrates that the vertical eddy fluxes proportional to $\overline{w'T'}\,\overline{T}_z$ (absent in the scalar computations) are much smaller than the horizontal fluxes $\overline{v'T'}\,\overline{T}_y$ so that the *eddy fluxes* are not along the mean *isopycnal slopes*. Instead, the horizontal eddy fluxes within the thermocline experience diffusion,

which tends to reduce their variance. Thus, the eddies are not adiabatic. A ''surface layer'' where the eddies are diabatic is necessary to close the mass transport circulation, even in more general contexts that include regions of adiabatic eddies, for example, the atmospheric boundary layer–troposphere system (Held and Schneider 1999). In our system, the thermocline and the surface layer coincide.

7. Energetics and scaling

In order to determine the dependence of the amplitude of the eddies on the external parameters, we examine the global energy balance in the statistical equilibrium. According to Paparella and Young (2002), when the only energy source is provided by the specification of the temperature at the top, the global energy balance is

$$\nu \int_0^H \langle \|\nabla \mathbf{u}\|^2 \rangle \, dz + \nu_6 \int_0^H \langle \|\nabla^2 \nabla \mathbf{u}\|^2 \rangle \, dz = \kappa g \alpha \langle T|_{z=H} - T|_{z=0} \rangle, \tag{62}$$

where $\|\nabla \mathbf{u}\|^2 \equiv \nabla u \cdot \nabla u + \nabla v \cdot \nabla v$ is the deformation ($\mathbf{u}$ denotes the horizontal velocity). The left-hand side of (62) is the dissipation of KE and the right-hand side is the source of PE: in steady state these two terms must balance. As explained in Paparella and Young (2002), the energy balance (62) implies that the energy dissipation vanishes in the limit of zero viscosity (holding Pr fixed) so that the boundary-forced system that we are studying is not strictly turbulent.[1] This contrasts with systems with energy input rate independent of ν and κ for which the usual arguments leading to the Kolmogorov spectrum apply.

For a shallow system with isotropic viscosity the deformation, $\|\nabla \mathbf{u}\|^2$ is dominated by the vertical derivatives. For our specific choice of forcing the area-averaged surface temperature vanishes so that (62) is very well approximated by

$$\nu \int_0^H \langle u_z^2 + v_z^2 \rangle \, dz + \nu_6 \int_0^H \langle \|\nabla^2 \nabla \mathbf{u}\|^2 \rangle \, dz = - \kappa g \alpha \langle T|_{z=0} \rangle. \tag{63}$$

The dominant contribution to the first integral on the left-hand side of (63) may come from one of two regions: either the bottom Ekman layer or the thermocline. We find that the relative importance of the two regions depends on the Prandtl number. The contribution to the energy dissipation by the hyperviscosity comes from the scales at the grid size and, although not negligible, is always smaller than the viscous term: hyperviscosity is hereinafter omitted from the discussion.

[1] One definition of turbulence is that the energy dissipation is nonzero in the limit of vanishing ν and κ.

a. Ekman-layer regime

When the Prandtl number is not too large, the energy dissipation, defined as

$$\varepsilon \equiv \nu \int_0^H \langle u_z^2 + v_z^2 \rangle \, dz, \tag{64}$$

is dominated by the contribution of the bottom Ekman layer, so that (64) is approximately

$$\varepsilon \approx \varepsilon_{\mathrm{BL}} \equiv \nu \int_0^{\mathrm{TBL}} \langle u_z^2 + v_z^2 \rangle \, dz, \tag{65}$$

where the upper limit of integration is the top of the boundary layer. The bottom Ekman layer velocities are determined by the barotropic component of the eddy flow.

In this regime bottom drag is the essential equilibration mechanism for the baroclinic eddies: energy is transferred from the baroclinic to the barotropic eddies and the latter are dissipated in the bottom Ekman layer. Because the thickness of the Ekman layer is $\delta = \sqrt{2\nu/f}$, the dissipation scales as

$$\varepsilon_{\mathrm{BL}} \sim \sqrt{\nu f} V'^2. \tag{66}$$

Using the scaling (66) in (63) and assuming that the abyssal temperature is the minimum surface temperature, we find

$$V' \sim \left(\frac{\kappa}{\mathrm{Pr} f} \right)^{1/4} (g \alpha \Delta T)^{1/2}. \tag{67}$$

The relations in (61) and (67) therefore imply that the depth of the thermocline scales as

$$h \sim \sqrt{L} (\kappa^3 \mathrm{Pr} f)^{1/8} (g \alpha \Delta T)^{-1/4}. \tag{68}$$

Although in this regime we do not have a quantitative prediction for the KE of the baroclinic flow, our scaling of the dissipation (66) implies that most of the eddy KE is in the barotropic mode.

b. Thermocline regime

For larger Pr dissipation occurs within the thermocline itself so that

$$\varepsilon \approx \varepsilon_{\mathrm{TH}} \equiv \nu \int_{\mathrm{TBL}}^H \langle u_z^2 + v_z^2 \rangle \, dz, \tag{69}$$

where the integral is performed over all depths above the bottom boundary layer.[2]

Because the vertical scale of the eddies coincides with the thermocline depth h, the dissipation scales as

$$\varepsilon_{\mathrm{TH}} \sim \nu v'^2 / h, \tag{70}$$

[2] The thermocline and the bottom boundary layer are always well separated so that there is no ambiguity in the definitions of $\varepsilon_{\mathrm{BL}}$ and $\varepsilon_{\mathrm{TH}}$.

where v' is the typical amplitude of the *baroclinic* eddy velocity.

To determine h from (61) we must relate the baroclinic velocity v' to the barotropic velocity V'. To do this we invoke the vertically averaged vorticity equation, whose derivation is given in appendix B:

$$\overbrace{\zeta_t}^{O[V'/(lt_{\text{eddy}})]} = \overbrace{\frac{1}{H}\int [(\partial_y^2 - \partial_x^2)uv + \partial_x\partial_y(u^2 - v^2)]\, dz}^{O[v'^2 h/(Hl^2)]} - \frac{\sqrt{\nu f}}{2H}\zeta + \nu\nabla^2\zeta. \quad (71)$$

Above, $\zeta \equiv V_x - U_y$ is the vorticity of the barotropic flow. In this regime, the bottom drag is negligible, and the nonlinear interactions among baroclinic contributions to the first term on the right hand side of (71) are the source of barotropic vorticity (Salmon 1980). Assuming that the time scale is the eddy-turnover time, $t_{\text{eddy}} = l/V'$, and that the length scales of baroclinic and barotropic eddies coincide, we find

$$V'^2 \sim v'^2 h/H \sim g\alpha\Delta T h^2/(H\text{Pr}). \quad (72)$$

In this regime the KE of the baroclinic and barotropic eddies are of the same order, a prediction that can be tested with the numerical calculations.

Using the relation (72) in (61) leads to

$$h \sim (\kappa L)^{1/3}\left(\frac{H\text{Pr}}{g\alpha\Delta T}\right)^{1/6}. \quad (73)$$

In (68) and (73) we have two different predictions for the dependence of the thermocline depth h on external parameters.

The scaling (73) is valid as long as the dissipation effected by the baroclinic flow in the thermocline dominates the bottom-boundary layer dissipation; that is, as long as

$$v^2 \gg hV'^2\sqrt{\frac{f}{\nu}}. \quad (74)$$

Using (72) and (73) this constraint demands that

$$\kappa \ll (g\alpha\Delta T)^2\left(\frac{H}{L}\right)^4\frac{\text{Pr}}{f^3}. \quad (75)$$

This corresponds to the following ordering of the nondimensional parameters:

$$\text{Ek} \ll \text{RoPr}. \quad (76)$$

Thus deep domains, with large Prandtl number, and large thermal gradients, should follow the thermocline-dissipation scaling (73).

c. The numerical results

An a posteriori attribution of each numerical computation to either regime follows from the evaluation of the relative magnitude of ε_{BL} and ε_{TH}. Figure 12 shows the ratio $\varepsilon_{\text{TH}}/\varepsilon_{\text{BL}}$ for all numerical computations performed to date. In the experiments with Pr = 10 the dissipation is dominated by the bottom boundary layer contribution. In the runs with Pr = 50 and H = 2000 m the dissipation is approximately equipartioned between the thermocline and the bottom boundary layer while, when H = 4000 m, the dissipation occurs predominantly in the thermocline as predicted by (76).

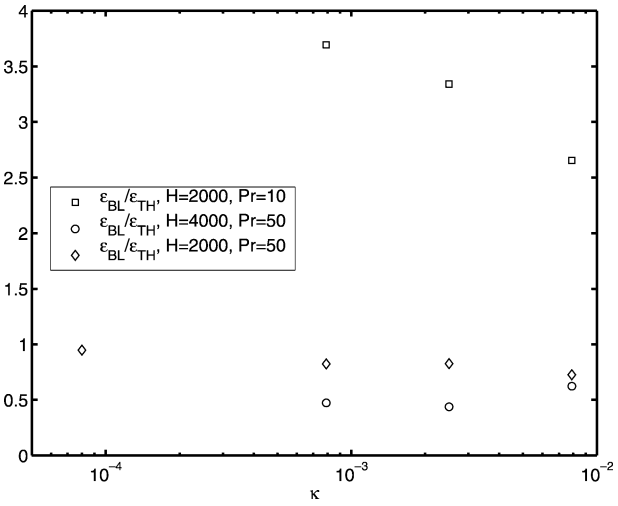

FIG. 12. The ratio of energy dissipation in the bottom boundary layer and in the thermocline, $\varepsilon_{\text{BL}}/\varepsilon_{\text{TH}}$, as a function of κ, for two values of Pr and H. All other parameters are as in Table 1.

To illustrate the validity of the proposed scalings we show in Fig. 13 the barotropic and baroclinic KE as a function of κ for two values of Pr and two values of H. The prediction that the barotropic KE increases as $\sqrt{\kappa}$ is satisfied for the series at Pr = 10, H = 2000 m, and in this regime the baroclinic KE (asterisks) is less than the barotropic KE (squares). The ordering (76) suggests that the dependence $\kappa^{2/3}$ for both the barotropic and baroclinic KE should be obtained for the two series at Pr = 50 and especially for the deeper domain. Indeed, the scaling (72) with (73) is well satisfied by the two series at Pr = 50.

Figure 14 shows the dependence of h on κ, Pr, and H. Both scalings are consistent with our numerical results, although the dependence (68) does a better job at collapsing all the data onto one line.

Last, we note that in the ''thermocline regime'' the Richardson number, $\text{Ri} \equiv N^2/v_z^2$, is of order

$$\text{Ri} \sim \frac{g\alpha\Delta T h}{v'^2}, \quad (77)$$

and thus scales as the Prandtl number as in the symmetric steady state [cf. (36)], (we have assumed that the relevant vertical stratification is $g\alpha\theta_z$).

The proposed scalings are summarized in Table 2, and we find that they are in reasonable agreement with the computations performed to date.

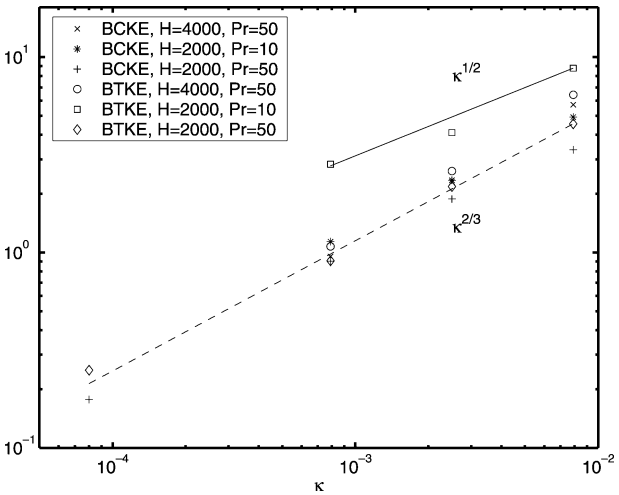

FIG. 13. The total barotropic (BTKE) and baroclinic (BCKE) KE per unit area ($m^3\ s^{-2}$) as a function of κ, for two values of Pr and H. The barotropic velocity is defined as the vertically averaged velocity, and the baroclinic one is the difference between the total and the barotropic velocity. The KE are divided by the actual abyssal temperature, $-T|_{z=0}$, since the latter depends weakly on κ. The solid line shows a $\kappa^{1/2}$ slope and the dashed line a $\kappa^{2/3}$ slope. All other parameters are as in Table 1.

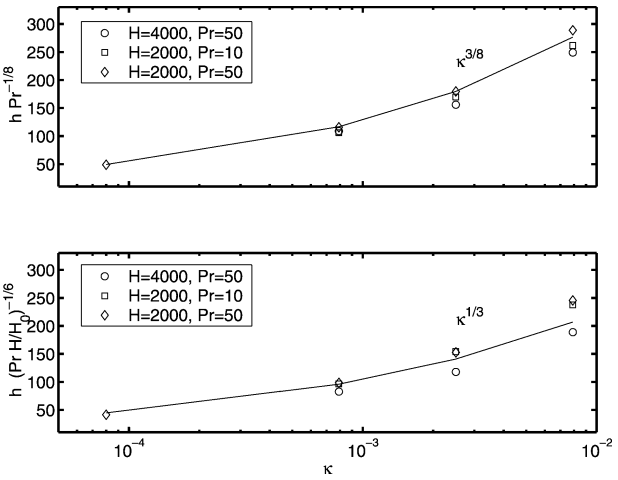

FIG. 14. The depth of the thermocline in meters, defined in (52), (top) weighted by $\mathrm{Pr}^{-1/8}$ and (bottom) weighted by $(\mathrm{Pr}H/H_0)^{-1/6}$ as a function of the diffusivity κ. The values of Pr and H are given in the legend, and $H_0 = 2000$.

The assumption of equal length scales for the baroclinic and barotropic eddies, made just before (72), is perhaps the weakest link in our chain of hypotheses. Figure 15 shows the normalized spectra of the barotropic and baroclinic KE for three calculations at different values of κ, all with $\mathrm{Pr} = 50$ and $H = 2000$ m. We define the energy spectra as

$$\langle U'^2 + V'^2 \rangle = \int_0^\infty \mathcal{E}_{\mathrm{BT}}(k, t)\, dk \quad \text{and} \tag{78}$$

$$\langle u'^2 + v'^2 \rangle = \int_0^\infty \mathcal{E}_{\mathrm{BC}}(k, z, t)\, dk. \tag{79}$$

Each spectrum is normalized so that the total area is unity and it is plotted against the scale $k^* \equiv k/k_B$, where k_B is the wavenumber at the peak of the spectrum, defined as

$$k_B = \int_0^\infty k\mathcal{E}\, dk. \tag{80}$$

Although all spectra collapse almost to a single curve, the insert shows that the peak wavenumber of the barotropic KE spectrum (the star markers in Fig. 15) does not coincide with the peak wavenumber of the baroclinic KE spectrum (the circle markers in Fig. 15). Therefore, the assumption that the scale of the barotropic and the baroclinic eddies coincide is not well verified by our direct simulations. However, an alternative scaling based on the commonly used argument stating that the barotropic eddies undergo an inverse cascade governed by the Kolomogorov spectrum, which is arrested at large scales by bottom friction (Smith et al. 2002), does not

TABLE 2. Summary of the scaling laws obtained in this work, compared with those of the laminar regime; h is the thermocline depth, and H is the full depth of the ocean. The question mark indicates that the scaling provides no prediction.

Laminar balance (Welander 1971)	Eddy balance (this work)	
	$h \sim \left(\frac{\kappa L}{V'}\right)^{1/2}$	
$h \sim \left(\frac{\kappa L}{\overline{v}}\right)^{1/2}$	$\varepsilon_{\mathrm{BL}} \gg \varepsilon_{\mathrm{TH}}$	$\varepsilon_{\mathrm{BL}} \ll \varepsilon_{\mathrm{TH}}$
$\overline{v} \sim \frac{g\alpha\Delta T H}{fL}$	$V' \sim \left(\frac{\kappa}{\mathrm{Pr}f}\right)^{1/4}(g\alpha\Delta T)^{1/2}$	$V' \sim v'\left(\frac{h}{H}\right)^{1/2} \sim h\left(\frac{g\alpha\Delta T}{H\mathrm{Pr}}\right)^{1/2}$
$h \sim \left(\frac{\kappa f L^2}{g\alpha\Delta T}\right)^{1/3}$	$h \sim L^{1/2}\kappa^{3/8}\frac{(\mathrm{Pr}f)^{1/8}}{(g\alpha\Delta T)^{1/4}}$	$h \sim (L\kappa)^{1/3}\left(\frac{H\mathrm{Pr}}{g\alpha\Delta T}\right)^{1/6}$
	$\mathrm{BTKE} \sim \left(\frac{\kappa}{\mathrm{Pr}f}\right)^{1/2} g\alpha\Delta T H$	$\mathrm{BTKE} \sim \left(\frac{L\kappa g\alpha\Delta T}{\mathrm{Pr}}\right)^{2/3} H^{1/3}$
	BCKE ~ ?	BCKE ~ BTKE

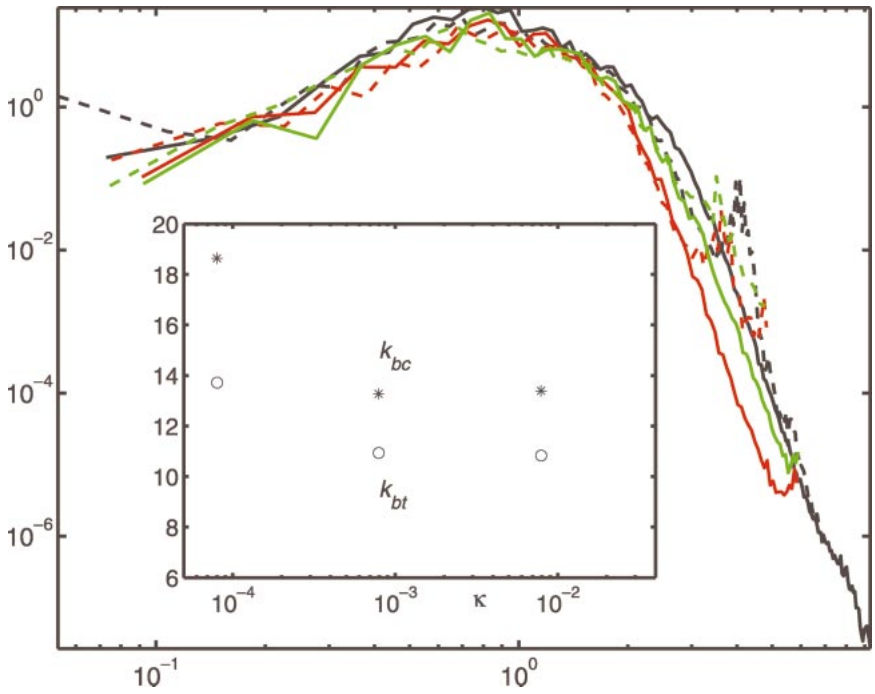

FIG. 15. The normalized spectra of barotropic KE, $\mathcal{E}_{BT}$, (solid) and baroclinic KE at $z = 1895$ m, $\mathcal{E}_{BC}$, (dashed) for three simulations all at Pr = 50 and $H = 2000$ m. The abscissa is the wavenumber scaled by the peak wavenumber of each spectrum, $k^* = k/k_{bc}$ or $k^* = k/k_{bt}$. The black lines are at $\kappa = 8 \times 10^{-5}$, the red lines are at $\kappa = 8 \times 10^{-4}$, and the green lines are at $\kappa = 8 \times 10^{-3}$. The inset shows the peak wavenumbers of each spectrum in units of $2\pi/L$ for the three values of κ: the stars are for the barotropic energy, k_{bt}, and the circles are for the baroclinic energy, k_{bc}.

fit with the data at all. This is because diffusion (and thus viscosity at fixed Pr) is important in the cascade; the usual inviscid arguments leading to the Kolmogorov spectrum are inapplicable here. The spectra clearly show injection of baroclinic energy at high wavenumbers characterized by a narrow peak near the deformation radius.[3] Thus, an inverse cascade indeed transfers energy upward from the linearly unstable wavenumber toward larger scales.

In conclusion we regard the dependence on the Prandtl number as the most convincing evidence that in the eddying regime the scaling differs substantially from Welander's laminar scaling [cf. (68) and (73) with (11)]. However, the scalings proposed here might be revised and improved by better understanding the factors that determine the length scales of the eddies.

8. The horizontally averaged temperature

The considerations in sections 6 and 7 apply only to the vertical scale h defined in (52), which characterizes $\theta(y, z)$. We turn now to the vertical structure of the horizontally averaged temperature, $\langle T\rangle(z)$.

Obviously, the scalar model of section 6 cannot determine the horizontally averaged stratification because $\langle T\rangle(z)$ is balanced by the small *vertical* eddy fluxes, associated with the horizontal divergence of the ageostrophic velocity [as in (1)]. Several terms contribute to the time-dependent ageostrophic vertical velocity, including friction, diffusion, and the (poorly) resolved hydrostatic convection, which strongly depends on the horizontal resolution, because it preferentially operates at horizontal scales much smaller than our grid size (Marshall and Schott 1999).[4] Thus, it is difficult to single out a dominant mechanism for the vertical eddy heat flux and provide a scaling argument.

The numerical results, shown in Fig. 16, suggest that the vertical scale of the mean stratification h_0, defined as

$$h_0 \equiv \left[\int_0^H \langle T(z) - T(0)\rangle^2\, dz \Big/ \int_0^H \langle T_z\rangle^2\, dz\right]^{1/2}, \quad (81)$$

decreases as $\kappa^{1/3}$ and, unlike the vertical scale of the zonally varying stratification, h, it is approximately independent of the Prandtl number. Because the numerical

[3] The two-dimensional spectrum, not shown here, illustrates that the high-wavenumber peak is near the lowest wavenumbers in the y direction but at high wavenumbers in the x directions.

[4] Specifically, we find that without convective adjustment, the bottom temperature decreases toward the minimum surface value as the horizontal resolution increases.

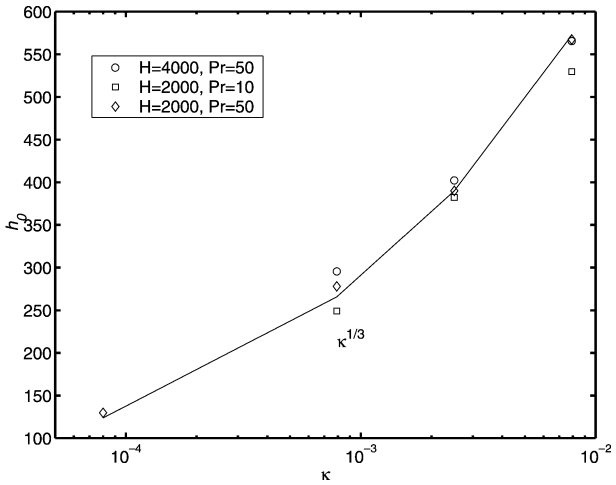

FIG. 16. The vertical scale of the mean stratification in meters, h_0 defined in (81), as a function of the diffusivity κ. The solid line shows the slope $k^{1/3}$.

results do not support a clear dependence on the depth of the domain H, dimensional analysis suggests that Welander's scaling (10) might apply for the horizontally averaged stratification, although for entirely different reasons than those originally advanced.

9. Summary and discussion

Our study focuses on the role of baroclinic eddies in effecting heat fluxes that balance diapycnal mixing, and thus establishing a thermocline, that is, a region containing the temperature gradients imparted to the ocean surface by the atmosphere. In order to study this thermocline formation in its simplest setting, we have excluded the processes that would generate a mean meridional circulation, such as wind stress and lateral boundaries.

We find that the eddy fluxes of heat that balance the diabatic fluxes are mainly due to the barotropic component of the eddies, rather than to the baroclinic eddy velocities. This is a well-known result in the context of the two-layer, quasigeostrophic model (Salmon 1980, Larichev and Held 1995), and we find that it applies even in the continuously stratified limit studied here, where the mean stratification, associated with the horizontally averaged temperature $\langle T\rangle(z)$, is *smaller* than the latitudinally varying stratification, related to the zonally averaged temperature $\theta(y, z)$. Unlike the quasigeostrophic systems analyzed by Salmon (1980); and Larichev and Held (1995), we do not have a traditional turbulent cascade: here diffusion and viscosity determine the energy generation rate. As a result, the properties of the statistically steady state depend on viscosity and the Kolmogorovian arguments based on inertial cascades are inapplicable.

The accuracy of the scalar model of section 6 confirms the predominance of the barotropic eddies, that is, the vertically averaged and horizontally nondivergent flow, in transporting heat. Thus eddy transport is horizontal rather than along isopycnals. Because the vertical eddy fluxes are small compared to the horizontal eddy fluxes, the eddies are diabatic, and in our eddy-driven thermocline diapycnal diffusion enters the dominant balance for both the time-dependent fluctuations and the zonal average. The scalar model confirms a peculiar picture of a time-dependent temperature field that is *advected horizontally* and *diffused vertically*.

Because the equilibrium amplitude of the eddies decreases with increasing viscosity, the depth of the thermocline depends both on κ and ν. The viscosity parameter does not appear in the laminar theory of Welander (1971). It is also noteworthy that in both of our scalings the dependence on the temperature difference ΔT and on the horizontal domain size L does not occur solely in the combination $\Delta T/L$ as in Welander's theory. This is because the total potential energy of the system depends on the difference between the top and the bottom temperature, which enters the scaling through the energy constraint. However, the dependences on the temperature difference and on the horizontal domain size have not been tested in our series of calculations.

Our results indicate that baroclinic eddies with scales from 50 to 100 km can maintain a thermocline against diapycnal diffusion, which is of the same order of magnitude as what would be obtained in a closed basin using Welander's laminar theory. In both cases, using observed midocean values of diapycnal diffusivity, the thermocline is too shallow: stratification is observed throughout the deep and abyssal ocean, while our thermocline is only 100 m deep for our smallest diffusivity. Thus, it is likely that the interaction of eddies and the mechanical forcing imparted by the wind allows the surface gradients to penetrate much deeper than with buoyancy forcing alone.

Acknowledgments. Funding for this research is provided by the U.S. Department of Energy Climate Change Prediction Program and the Italian Ministry of Research through the program ''SINAPSI/Ecosistemi Marini.'' We acknowledge the Center for Computational Sciences–Climate and Carbon Research (CCS–CCR) at Oak Ridge National Laboratory for computational resources used in support of this project. We benefited from discussions with Bill Young, Rick Salmon, and Piero Malguzzi, and from the useful suggestions provided by two anonymous referees.

APPENDIX A

The Numerics

The hydrostatic Boussinesq equations (12) are written in finite-difference form on the Arakawa C grid. The vertical differencing, on *nz* levels, is Lorenz type; that is, u, v, p, and T are on the same levels zp_k, while w is

TABLE A1. Summary table of the physical and numerical parameters used in the computations. The symbols are defined in the text.

Pr	H (m)	κ ($m^2\ s^{-1}$)	nz	A	ν_6 ($m^6\ s^{-1}$)	N
50	2000	8.0×10^{-5}	75	6.75	9×10^{15}	256
50	2000	7.9×10^{-4}	30	6.8	3×10^{17}	128
50	2000	2.5×10^{-3}	30	6.8	3×10^{17}	128
50	2000	7.9×10^{-3}	29	7.0	3×10^{17}	128
50	4000	7.9×10^{-4}	27	7.0	3×10^{17}	128
50	4000	2.5×10^{-3}	80	6.8	3×10^{17}	128
50	4000	7.9×10^{-3}	27	6.8	3×10^{17}	128
10	2000	7.9×10^{-4}	82	8.0	9×10^{15}	256
10	2000	2.5×10^{-3}	50	8.0	3×10^{17}	128
10	2000	7.9×10^{-3}	40	8.0	3×10^{17}	128

on the levels zw_k intermediate between zp_{k-1} and zp_k (Arakawa and Moorthi 1988).

The vertical grid spacing is uniform in a transformed variable s defined by

$$s \equiv z - \frac{H}{A}\sin\left(2\pi\frac{z}{H}\right). \tag{A1}$$

With the constraint, $A > 2\pi$, the physical grid interval can be stretched near the center of the domain, where little resolution is needed, and reduced near the top and bottom boundaries where the Ekman layers are located. This formulation maintains second-order accuracy of the vertical differentiation (Marti et al. 1992).

We use a second-order, three time-levels stepping scheme (leapfrog–trapezoidal), with the advective terms calculated at the central time, the horizontal diffusion, and viscosity terms at the previous time and the vertical diffusion and viscosity terms treated with a Crank–Nicholson implicit scheme (one-half at the forward time and one-half at the previous time). The time step is $\Delta t =$ 900 s for all runs at 128^2 grid points and $\Delta t = 450$ s for the computations at 256^2 grid points.

The rigid-lid top and bottom boundary conditions imply an integral constraint on the horizontal divergence, enforced by solving an elliptic equation for the vertically averaged pressure. See Fantini (1999) for details.

Table A1 shows the physical and numerical parameters for all the experiments performed, and N denotes the number of grid points in each horizontal direction. Here we note the typical dissipation time scales associated with the viscous parameters: the spindown time, $t_{\rm Ek} \equiv \delta H/\nu$, ranges from 5 to 100 days; the hyperviscosity damping time on the grid scale, $t_{\nu 6} \equiv (dx)^6/\nu_6$, ranges from 5 to 10 days; and the viscosity damping time on the grid scale, $t_\nu \equiv (dx)^2/\nu$, ranges from 5 to 500 years.

APPENDIX B

The Vertically Averaged Vorticity Equation

Subtracting the y derivative of the x momentum equation from the x derivative of the y momentum equation in (12) we obtain

$$(v_x - u_y)_t + (\partial_x^2 - \partial_y^2)uv + \partial_x\partial_y(u^2 - v^2) + \partial_z[(wv)_x - (wu)_y] - f(u_x + v_y) = \nu(v_x - u_y)_{zz} + \nu\nabla^2(v_x - u_y). \tag{B1}$$

Taking the vertical average, and using the incompressibility condition to eliminate the horizontal divergence, we arrive at

$$\zeta_t + H^{-1}\int_0^H [(\partial_x^2 - \partial_y^2)uv + \partial_x\partial_y(v^2 - u^2)]\,dz = \nu\nabla^2\zeta - H^{-1}\nu(v_x - u_y)_z|_{z=0}. \tag{B2}$$

Standard analysis of the bottom Ekman layer gives

$$(u + iv)_z|_{z=0} \approx \sqrt{\frac{f}{2\nu}}(1 + i)(u_I + v_I)|_{z=0}, \tag{B3}$$

where (u_I, v_I) indicates the interior velocity above the bottom boundary layer. Assuming that the interior velocity at the bottom is dominated by the barotropic component (U, V) we find

$$\nu(v_x - u_y)_z|_{z=0} \approx \sqrt{\frac{\nu f}{2}}(V_x - U_y). \tag{B4}$$

REFERENCES

Arakawa, A., and S. Moorthi, 1988: Baroclinic instability in vertically discrete systems. *J. Atmos. Sci.*, **45,** 1688–1707.

Doos, K., and D. Webb, 1994: The Deacon Cell and the other meridional cells of the Southern Ocean. *J. Phys. Oceanogr.*, **24,** 429–442.

Eady, E. T., 1949: Long waves and cyclone waves. *Tellus*, **1,** 33–52.

Fantini, M., 1999: Linear evolution of baroclinic waves in saturated air. *Quart. J. Roy. Meteor. Soc.*, **125,** 905–923.

Gill, A. E., 1982: *Atmosphere–Ocean Dynamics.* Academic Press, 662 pp.

——, J. S. A. Green, and A. J. Simmons, 1974: Energy partition in the large-scale ocean circulation and the production of mid-ocean eddies. *Deep-Sea Res.*, **21,** 499–528.

Held, I. M., and T. Schneider, 1999: The surface branch of the zonally averaged mass transport circulation in the troposphere. *J. Atmos. Sci.*, **56,** 1688–1697.

Henning, C., and G. K. Vallis, 2004: The effects of mesoscale eddies on the main subtropical thermocline. *J. Phys. Oceanogr.*, **34,** 2428–2443.

Karsten, R., H. Jones, and J. Marshall, 2002: The role of eddy transfer in setting the stratification and transport of a circumpolar current. *J. Phys. Oceanogr.*, **32,** 39–54.

Larichev, V. D., and I. M. Held, 1995: Eddy amplitudes and fluxes in a homogeneous model of fully developed baroclinic instability. *J. Phys. Oceanogr.*, **25,** 2285–2297.

Luyten, J., J. Pedlosky, and H. Stommel, 1983: The ventilated thermocline. *J. Phys. Oceanogr.*, **13,** 292–309.

Marshall, J., and F. Schott, 1999: Open-ocean convection: Observations, theory, and models. *Rev. Geophys.*, **37,** 1–64.

——, H. Jones, R. Karsten, and R. Wardle, 2002: Can eddies set ocean stratification? *J. Phys. Oceanogr.*, **32,** 26–38.

Marti, O., G. Madec, and P. Delecluse, 1992: Comment on ''Net diffusivity in ocean general circulation models with nonuniform

grids'' by F. L. Yin and I. Y. Fung. *J. Geophys. Res.*, **97,** 12 763–12 766.
Munk, W., 1966: Abyssal recipes. *Deep-Sea Res.*, **24A,** 1259–1262.
Paparella, F., and W. R. Young, 2002: Horizontal convection is non-turbulent. *J. Fluid Mech.*, **466,** 205–214.
Salmon, R., 1980: Baroclinic instability and geostrophic turbulence. *Geophys. Astrophys. Fluid Dyn.*, **15,** 165–211.
——, 1990: The thermocline as an ''internal boundary layer.'' *J. Mar. Res.*, **48,** 437–469.
Samelson, R. M., and G. K. Vallis, 1997: Large-scale circulation with small diapycnal diffusion: The two-thermocline limit. *J. Mar. Res.*, **55,** 223–275.
Smith, K. S., G. Boccaletti, C. C. Hennings, I. Marinov, C. Y. Tam, I. M. Held, and G. K. Vallis, 2002: Turbulent diffusion in the geostrophic inverse cascade. *J. Fluid Mech.*, **469,** 13–48.
Stommel, H., and J. Webster, 1962: Some properties of the thermocline equations in a subtropical gyre. *J. Mar. Res.*, **44,** 695–711.
Stone, P. H., 1966: On non-geostrophic baroclinic stability. *J. Atmos. Sci.*, **23,** 390–400.
Vallis, G. K., 2000: Large-scale circulation and production of stratification: Effects of wind, geometry, and diffusion. *J. Phys. Oceanogr.*, **30,** 933–954.
Weideman, J. A. C., and S. C. Reddy, 2000: A MATLAB differentiation matrix suite. *ACM Trans. Math. Software*, **26,** 465–519.
Welander, P., 1971: The thermocline problem. *Philos. Trans. Roy. Soc. London*, **270A,** 415–421.
Young, W. R., and G. Ierley, 1986: Eastern boundary conditions and weak solutions of the ideal thermocline equations. *J. Phys. Oceanogr.*, **16,** 1884–1900.